Sensors and Actuators B 188 (2013) 533–539

Contents lists available at ScienceDirect

Sensors and Actuators B: Chemical

journal homepage: www.elsevier.com/locate/snb

# Facile synthesis of highly stable and porous $Cu_2O$/CuO cubes with enhanced gas sensing properties

Li-Jing Zhou [a], Yong-Cun Zou [a], Jun Zhao [a], Pei-Pei Wang [a], Liang-Liang Feng [a], Li-Wei Sun [a], De-Jun Wang [a,b], Guo-Dong Li [a,*]

[a] State Key Laboratory of Inorganic Synthesis & Preparative Chemistry, College of Chemistry, Jilin University, Changchun 130012, PR China
[b] Department of Chemistry, Tsinghua University, Beijing 100086, PR China

ARTICLE INFO

*Article history:*
Received 26 May 2013
Received in revised form 13 July 2013
Accepted 16 July 2013
Available online xxx

*Keywords:*
$Cu_2O$
CuO
Precursor
Gas sensor
Acetone

ABSTRACT

In this work, highly stable and porous $Cu_2O$/CuO cubes have been successfully synthesized by the calcination of the precursor at different temperatures (350 °C, 450 °C and 550 °C). The precursor which consists of cupric oxalate and cubic $Cu_2O$ was obtained by a one-step hydrothermal route with the help of ethylene glycol. The chemical composition and structure of the products were confirmed by powder X-ray diffraction, scanning electron microscopy, transmission electron microscopy and X-ray photoelectron spectroscopy. It is found that the cube is composed of nanoparticles with diameters around several dozens of nanometers and the calcination temperature has great influence on the size, the amount of $Cu_2O$ and the surface area of the final products. The gas sensing ability of the as-synthesized porous $Cu_2O$/CuO cubes was investigated toward a series of toxic organic molecules, in which the sample calcined at 350 °C exhibits higher sensing response to acetone. The higher sensing response of this sample might be attributed to the heterostructure of CuO and $Cu_2O$ and the relatively high surface area.



## 1. Introduction

With the remarkable development of science and technology, environmental pollution, especially air pollution, both indoors and outdoors, has become a universal problem [1]. Therefore, it has provided the impetus to carry out fundamental and applied research on sensors with the ability to detect polluting gases. Among these sensors, metal-oxide semiconductor gas sensors have become promising sensors for their unique advantages, such as cost-efficiency, short response time, wide range of target gases and long lifetime, all of which are of the essence to industrial application and civil use [2]. And great efforts have been devoted to obtain metal-oxide semiconductor materials for gas sensors via various methods [3–11].

It is well known that copper oxides (CuO and $Cu_2O$) are typical p-type semiconductors and are widely used for gas sensors. And many methods have been developed for the synthesis of nanostructured Cu-based materials. Up to now, various nanostructured Cu-based materials such as nanopaticals, nanorods, nanoribbons, nanofilms, nanospheres, hollow mecrospheres and hierarchical nanostructures have been successfully synthesized [9–17]. The investigation on the morphology of material has attracted intense attention over the past decades for the great influence on the performance of a material, while porous materials have been extensively investigated due to high surface area and tunable pore size in the fields of catalysis, adsorption, gas sensing, separation, and so on. Such porous materials have been fabricated via various processes such as the vacuum assisted solvent evaporation method [18], co-evaporation of metal oxide powders [19], surfactant-mediated syntheses [20] and the soft/hard template method [21,22]. Nevertheless, these methods have a drawback in the requirement of vacuum system or the elimination of templates. As an effective way to prepare many porous materials, precursor method has attracted increasing interest. In consideration of the above promising applications of CuO and $Cu_2O$, porous CuO and $Cu_2O$ nanostructures have been synthesized by a precursor method. By using $Cu_2(OH)_2CO_3$ as a precursor, hierarchically porous CuO architectures were successfully fabricated via a hydrothermal route [17]. Wu et al. reported the detection of ethanol by wormlike CuO produced by Brochantite ($Cu_4(OH)_6SO_4$) tabular microspindles [23]. However, pure CuO is usually obtained by the precursor method. Nanocomposites have caused great attention for their unique and superior properties. Up to now, some $Cu_2O$/CuO composites have been reported as photocatalysts, photoanodes, ferromagnetic materials, whereas it is rarely reported for the detection of acetone at low temperature (150 °C) [17,24].

Herein, we successfully design a precursor for the preparation of porous $Cu_2O$/CuO architectures in the absence of any templates and

* Corresponding author. Tel.: +86 431 85168318.
*E-mail addresses:* lgd@jlu.edu.cn, lifind@21cn.com (G.-D. Li).

0925-4005/$ – see front matter © 2013 Elsevier B.V. All rights reserved.
http://dx.doi.org/10.1016/j.snb.2013.07.059

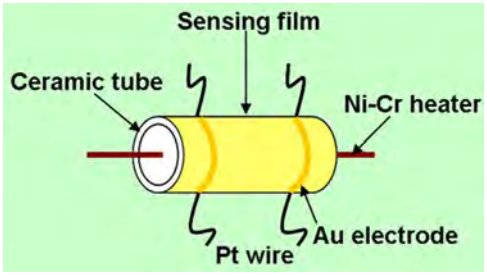


**Fig. 1.** Schematic structure of the gas sensor.

surfactants. By calcined at different temperatures (350 °C, 450 °C and 550 °C), porous $Cu_2O$/CuO cubes with different amount of $Cu_2O$ have been successfully synthesized. In addition, gas sensing performance was examined with acetone, benzene, methanol, ammonia and ethanol. After calcined at 350 °C, the porous $Cu_2O$/CuO gave the highest response to acetone at 150 °C and might become a promising gas sensor for the detection of acetone.

## 2. Experimental

### 2.1. Preparation of nanostructured $Cu_2O$/CuO cubes

$Cu(NO_3)_2{\cdot}3H_2O$ was purchased from Tianjin Guangfu Tech. Co., Ltd.; ethylene glycol was purchased from Beijing Chemical Factory. All of the chemicals were of analytical grade and were used without further purification. In a typical procedure, 2.71 g $Cu(NO_3)_2{\cdot}3H_2O$ was dissolved in 50 mL of solution which consisted of deioned water and ethylene glycol (volume ratio = 10:1). The solution was vigorously stirred at room temperature for 1 h to form homogeneous blue solution. The above solution was put in a 100 mL Teflon-sealed autoclave, which was then heated at 140 °C for 10 h. The blue green precipitate (the precursor) was obtained after the autoclave was cooled naturally to room temperature. The product was centrifuged, washed with deionized water and ethanol several times and dried in an oven at 60 °C for 12 h. Afterwards, the porous $Cu_2O$/CuO architectures were generated by subsequent calcination of the former precursor at different temperatures (350 °C, 450 °C and 550 °C) in a muffle furnace for 3 h. The as-prepared materials are designated S-350, S-450, S-550, respectively.

### 2.2. Characterization and gas sensor test

The powder X-ray diffraction (XRD) patterns were carried out on a Rigaku D/Max 2550 X-ray diffractometer using Cu K$\alpha$ radiation ($\lambda$ = 1.5418 Å). The scanning electron microscopy (SEM) images were taken on a JEOL JSM 6700F electron microscope, whereas the transmission electron microscopy (TEM) and high-resolution TEM (HRTEM) images were obtained on a Philips-FEI Tecnai G2S-Twin. The FT-IR spectra were acquired on a Bruker IFS 66v/S FTIR spectrometer. The X-ray photoelectron spectroscopy (XPS) was analyzed by an ESCALAB 250 X-ray photoelectron spectrometer with a monochromated X-ray source (Al K$\alpha$ $h\upsilon$ = 1486.6 eV). The thermogravimetric (TG) analysis for the precursor was performed in air on a NETZSCH STA 449 C TG thermal analyzer from 25 to 800 °C at a heating rate of 10 °C $min^{-1}$. The nitrogen adsorption and desorption isotherms were measured by a Micromeritics ASAP 2020M system. The temperature programmed desorption (TPD) was performed using an Automated Catalyst Characterization System (AutoChem II 2920).

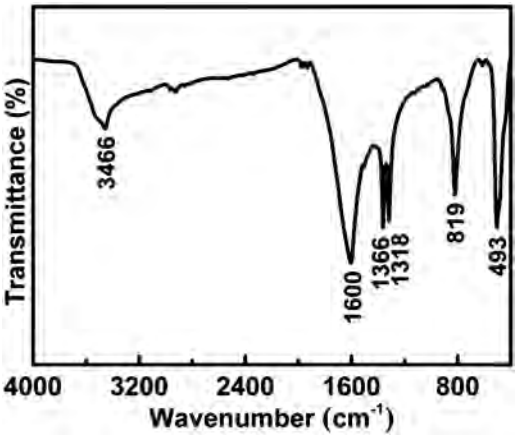


**Fig. 3.** IR spectrum of the precursor.

The product was mixed with ethanol to form a paste. The gas sensor was fabricated by coating viscous paste onto an alumina tube with a diameter of 1 mm and a length of 4 mm, which was positioned with a pair of Au electrodes and four Pt wires on both ends of the tube. A Ni–Cr alloy coil through the tube was employed as a heater to offer the operating temperature. The structure of the sensor is shown in Fig. 1.

Gas sensor tests were performed on a CGS-8 Gas Sensing Measurement System (Beijing Elite Tech Company Limited). The response is defined as the ratio $R_g/R_a$, where $R_g$ and $R_a$ are the electrical resistance of the sensor in the testing gas and in air, respectively. The response and recovery times are defined as the time taken by the sensor to achieve 90% of the total resistance change in the case of adsorption and desorption, respectively. For

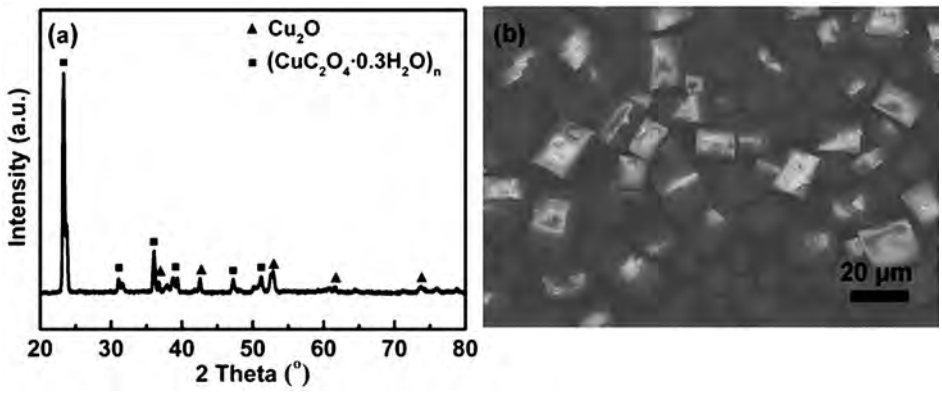


**Fig. 2.** (a) XRD pattern and (b) SEM image of the precursor.

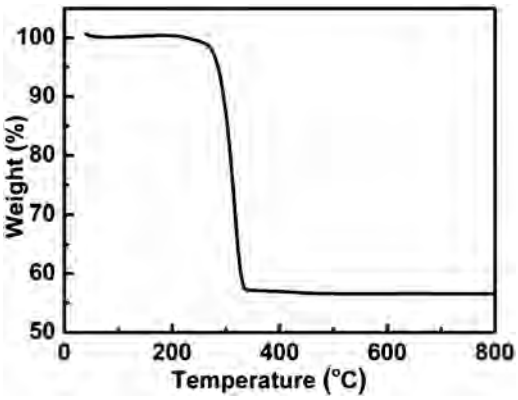


**Fig. 4.** TG analysis of the precursor.

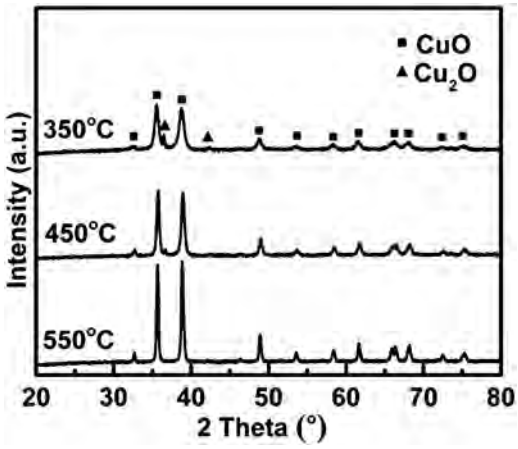


**Fig. 5.** XRD patterns of S-350, S-450, and S-550.

comparison, the sensing performance of commercial CuO was also tested.

## 3. Results and discussion

As shown in Fig. 2(a), the XRD pattern of the precursor can be attributed to cupric oxalate ($(CuC_2O_4{\cdot}0.3H_2O)_n$) and cubic $Cu_2O$ (JCPDS Card No. 65-3288) [25]. In other words, the precursor consists of cupper oxalate and a trace amount of $Cu_2O$. Furthermore, the SEM image of the as-prepared precursor is shown in Fig. 2(b). We can see that the precursor looks like a cube with rough surfaces and sharp edges. However, it is noted that the image is not very clear due to the existence of organic material. In order to further understand the structure of the precursor, IR was performed for the precursor. As shown in Fig. 3, the typical IR bands for cupper oxalate are nearly the same as the previous report [25]. The bands located at 1600 $cm^{-1}$ and 1366 $cm^{-1}$ are assigned to $\nu_{COO}{}^{-}$; 1318 $cm^{-1}$ and 819 $cm^{-1}$ are attributed to $\nu_{CO}$ and $\delta_{OCO}$; 493 $cm^{-1}$ is due to $\nu_{Cu\text{-}O}$ and $\delta_{OCO}$; the relatively weak peak at 3466 $cm^{-1}$ can be denoted as $\nu_{OH}$.

To further understand the thermal stability of the precursor, TG analysis of the precursor was employed. In Fig. 4, it is clear that a rapid weight loss is located in the range of 270–350 °C, which can be assigned to the decomposition of the precursor into the CuO and $CO_2$. The weight loss is about 44.09%, which is in agreement with the theoretical composition of the cupric oxalate. The difference is due to the trace amount of $Cu_2O$ in the precursor, and the ratio of $Cu_2O$ to $CuC_2O_4{\cdot}0.3H_2O$ is about 9.29%. According to the TG result, 350 °C, 450 °C and 550 °C were used as the calcination temperature of the products.

The typical XRD patterns of the as-synthesized products are shown in Fig. 5. It is clear that both CuO (JCPDS Card No. 48-1548)

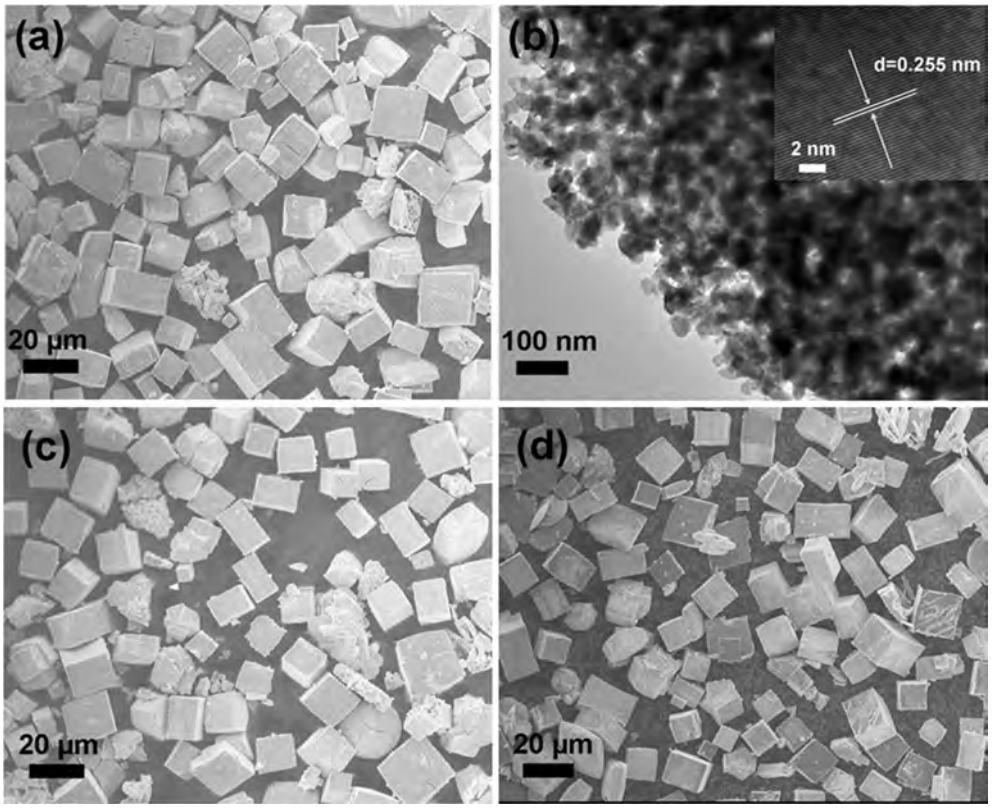


**Fig. 6.** (a) SEM image, (b) TEM image and HRTEM image (inset) of S-350, (c) SEM image of S-450, and (d) SEM image of S-550.

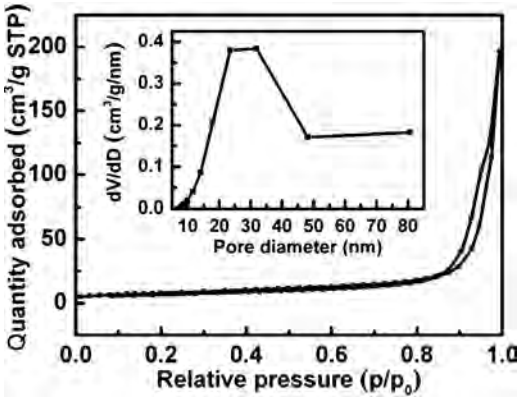


**Fig. 7.** $N_2$ adsorption–desorption isotherm and pore size distribution (inset) of S-350.

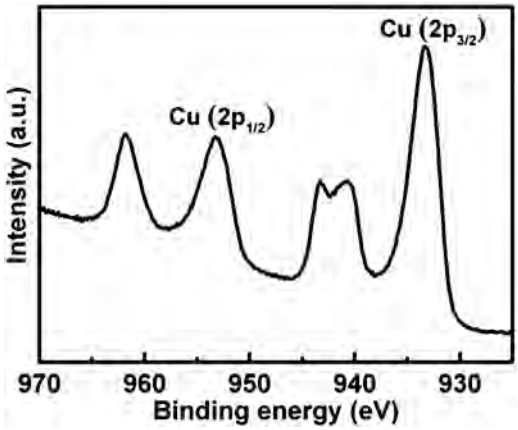


**Fig. 8.** XPS spectra of S-350.

and $Cu_2O$ (JCPDS Card No. 65-3288) patterns can be observed in the XRD pattern of S-350, S-450, while only CuO (JCPDS Card No. 48-1548) pattern is appeared in S-550. Moreover, the intensity of the diffraction peaks increases with the elevate calcination temperature. According to the previous study [26,27], the height of the characteristic diffraction peaks of CuO (1 1 1) and $Cu_2O$ (1 1 1) planes can be used for calculation of the relative content of $Cu_2O$ phase (wt%) in the porous CuO/$Cu_2O$ cubes. The relative content of $Cu_2O$ in the porous CuO/$Cu_2O$ cubes is about 36%, 22% and 0%, respectively.

The SEM image of S-350 is shown in Fig. 6(a), while, the SEM images of S-450 and S-550 are shown in Fig. 6(c) and (d). It is obvious that the morphologies are nearly the same as the precursor (Fig. 2(b)). The microstructure of S-350 is further confirmed by TEM as shown in Fig. 6(b). It is clear that the cube is composed of nanoparticles with a diameter around several ten nanometers. The HRTEM of the sample is shown in the inset of Fig. 6(b), and the lattice distance of the nanoparticles is about 0.255 nm, which is in good agreement with the (0 0 2) lattice fringe of monoclinic CuO. To further confirm the porous structure of S-350 architecture, the $N_2$ adsorption–desorption analysis is performed. The $N_2$ adsorption–desorption isotherm and BJH pore size distribution as the inset of the S-350 sample is shown in Fig. 7. The $N_2$ adsorption–desorption isotherm of S-350 is the type IV form, which is corresponding to the isotherm of typical mesoporous materials. The pore size is around 30 nm and is in consistent with the result of the TEM. In addition, the BET surface area of S-350 is 28 $m^2/g$, while the BET surface area is 9 and 5 $m^2/g$ for S-450 and S-550, and the average pore size is 50 and 60 nm, respectively.

XPS is a useful technique for analyzing the chemical nature of elements on the surface of compounds and studying the transition metal compounds having the localized valance d orbital [28]. To further confirm the structure of porous CuO/$Cu_2O$ cubes, XPS analysis of S-350 is performed. As shown in Fig. 8, the peaks located at 933.4 eV and 953.2 eV can be attributed to Cu $2P_{3/2}$ and Cu $2P_{1/2}$ of CuO, respectively. In addition, shake-up satellite peaks located at 940.6 eV, 943.2 eV and 961.8 eV cannot be ignored, which may be due to the open $3d^9$ shell of $Cu^{2+}$ [29]. The XPS peaks located at 932.6 eV and 952.4 eV are the characteristic signals of $Cu_2O$ for Cu $2P_{3/2}$ and Cu $2P_{1/2}$, respectively. It means that $Cu_2O$ is detected neither by XPS nor by HRTEM on the surface of S-350 and CuO is the main species on the surface of S-350.

As a promising candidate for gas sensing, Cu-based materials have been extensively studied for gas sensing [9–17]. It is well known that the gas response of a semiconductor gas sensor is closely related to the working temperature [30]. To determine the optimal operating temperature for porous CuO/$Cu_2O$ nanostructure, the response of S-350 to 500 ppm acetone in air is tested with an elevated temperature (Fig. 9). It is clearly seen that the highest response (9.7) appeared at 150 °C. Therefore, 150 °C is used as the optimal working temperature for the detection of acetone. The working temperature of S-350 sensor is much lower than previous reports [17,24]. Fig. 10(a) is the response–recovery curves of S-350 sensor to acetone with increasing concentration from 50 to 500 ppm. The resistance of the sensor increases abruptly for exposure to acetone and decreases rapidly for re-exposure to fresh air. Furthermore, it is noted that the resistance of the as-synthesized porous CuO/$Cu_2O$ increases when it is exposed to acetone vapor. It is because the density of positive holes in the p-type semiconductor would decrease when it is exposed to a reducing gas [31]. At the same time, the response–recovery curves of S-450 and S-550 are also tested (Fig. 10(b) and (c)). However, the responses are lower than that of S-350. For comparison, the sensing performance of commercial CuO has also been tested. The sensitivities of these sensors increase gradually with the increase of acetone at 150 °C which is shown in Fig. 10(d). For the concentrations of 50, 100, 200, 400, 500 ppm, the responses of S-350 are about 3.0, 4.4, 6.5, 9.0 and 9.9, respectively. Furthermore, it is obvious that the responses of S-350, S-450 and S-550 gas sensors exhibit distinctly higher sensitivity than that of the commercial CuO. The response of S-350 is about 2.3 times (4.3 times) as high as that of S-550 (commercial CuO) in the presence of 500 ppm acetone.

In addition, the response and recovery times are all key parameters for a gas sensor [32]. It is clear that the response times of S-350 to acetone are 2s, 2s, 1s, 1s and 1s, while the recovery times are 54s, 29s, 35, 32s and 25s for 50, 100, 200, 400, 500 ppm, respectively in Fig. 11(a). Gas sensing selectivity is extensively studied as a

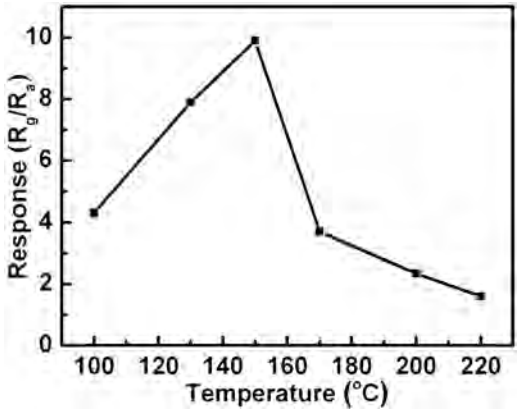


**Fig. 9.** Gas responses of S-350 measured at different operating temperatures to 500 ppm acetone.

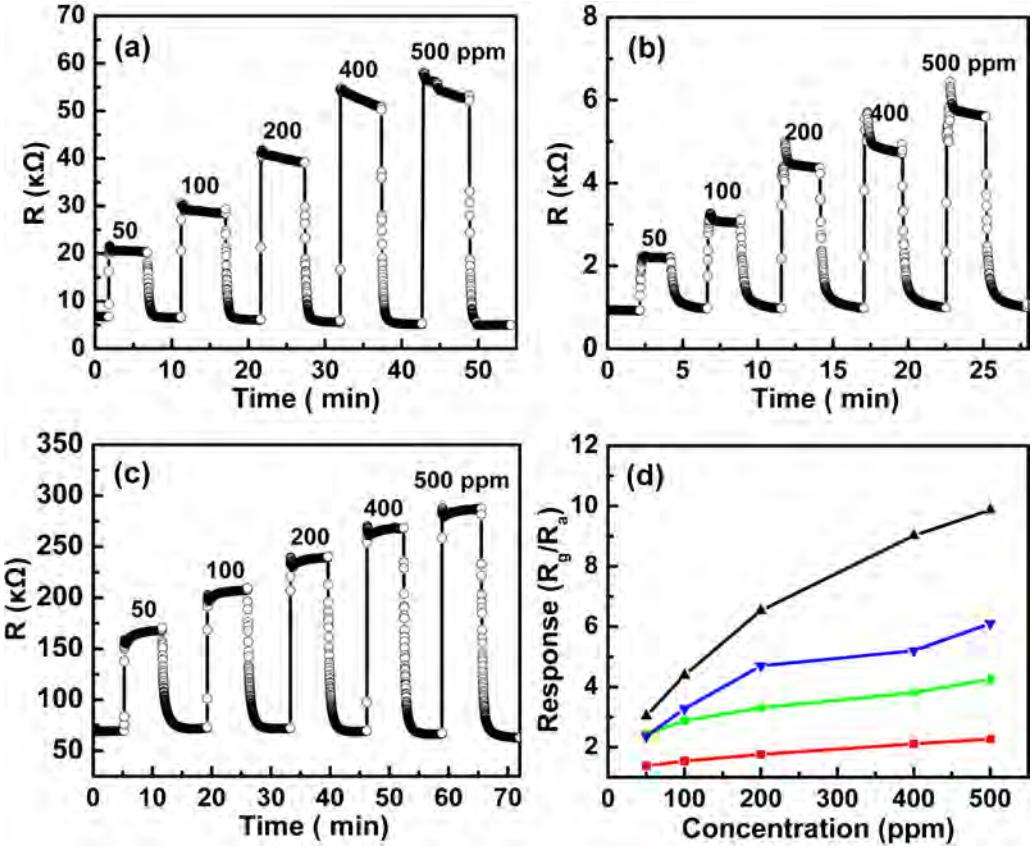


**Fig. 10.** Dynamic response–recovery curves of (a) S-350, (b) S-450, and (c) S-550 gas sensors to acetone with increasing concentrations. (d) Responses of S-350 (▲), S-450 (▼), S-550 (●), and commercial CuO (■).

crucial parameter for a sensor. To evaluate the selectivity of the sensor, other gases are used as target gas. As shown in Fig. 11(b), they are the responses of S-350 to 500 ppm acetone, benzene, methanol, ammonia and ethanol at 150 °C. It is clear that the sensor exhibits the highest response to acetone. Recently, CuO has been found to be a type of ferroelectric material that has a spontaneous electric dipole moment [33,34]. In addition, acetone has a much larger dipole moment than other gases [35]. Therefore, the strong interaction between porous $Cu_2O$/CuO cubes and acetone could be observed, leading to high sensing response to acetone. Temperature programmed desorption (TPD) is a useful method to understand the interaction between solid materials and absorbed species. The TPD spectra of acetone and other gases were obtained as shown in Fig. 12. For the TPD analysis, the desorption temperature depends on the strength of the interaction between $Cu_2O$/CuO and absorbed species. Usually, the peak at higher temperature is assigned to chemisorption first layer in the TPD spectra, whereas that at lower temperature is assigned to physisorption multi-layers covering the monolayer. The TPD peak area is in proportion to the amount of absorbed species. Thus, the amount of physisorption will be greater than that of chemisorption. And only the chemisorption can contribute to the sensing performance of a material. The higher the temperature of desorption is, the greater the interaction strength of $Cu_2O$/CuO and the absorbed species is. In the high temperature range, the desorption temperature of acetone, methanol and benzene center at 170 °C, 155 °C and 148 °C, respectively. And no obvious peak can be found in the TPD of ethanol in high temperature range. However, the relative low response to ammonia

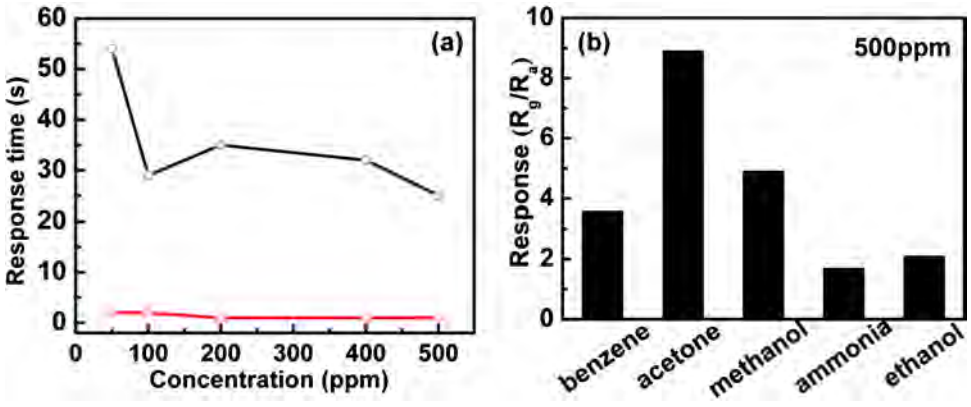


**Fig. 11.** (a) Response time (△) and recovery time (○) of S-350 and (b) responses of S-350 to five different gases (500 ppm) at 150 °C.

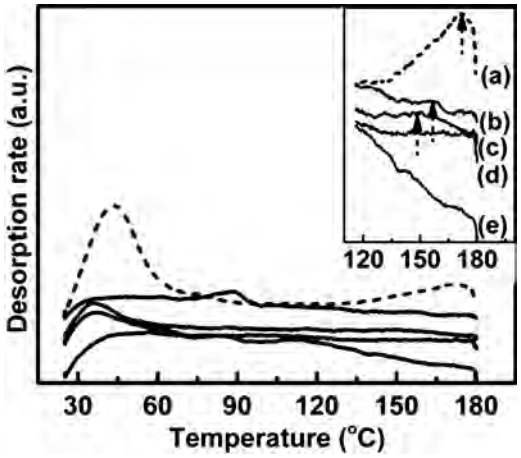


**Fig. 12.** Temperature programmed desorption (TPD) spectra of (a) acetone, (b) methanol, (c) benzene, (d) ethanol, and (e) ammonia of S-350.

may be attributed to the different mechanism [36]. The very weak coordinated bonds could be formed between ammonia and Cu of $Cu_2O$/CuO at 150 °C, leading to the much lower response. According to the TPD analysis, the interaction strength between porous $Cu_2O$/CuO cubes and the absorbed species are in the following order: acetone > methanol > benzene > ethanol > ammonia, which is in agreement with the order of sensing selectivity.

As we all known, both CuO and $Cu_2O$ are p-type semiconductors and the gas sensing mechanism of Cu-based gas sensors belongs to the surface controlled mode which probably involves serial reactions: adsorption–oxidation–desorption [10]. When the sensor is exposed to air, oxygen molecules would be adsorbed on the surface of porous $Cu_2O$/CuO cubes to generate $O^-$, $O_2^-$ and $O^{2-}$, leading to the increase of hole concentration and the decrease of the resistance. When it is exposed to acetone, acetone is oxidized to $CO_2$ and $H_2O$ by the absorbed oxygen species on the surface of the sensor, and the electrons go back to the valence band, decreasing the concentration of holes, and increasing the resistance. Then, the sensor breaks away from the surface acetone and restores to the original state in air. It is known that $Cu_2O$ is a direct band gap semiconductor, while CuO is an indirect band gap semiconductor [37]. When the sensor composed of $Cu_2O$ and CuO is exposed to air, more oxygen molecules will be adsorbed on the surface of porous $Cu_2O$/CuO cubes to generate $O^-$, $O_2^-$ and $O^{2-}$ and the resistance decreases more, leading to the improvement of gas sensing. The surface relative $O_{ads}/(O_{ads}+O_{latt})$ molar ratio was also studied by XPS [38]. The peak located at 529.9 eV is attributed to lattice oxygen ($O_{latt}$) and the board peak centered at 531.4 eV is denoted as surface adsorbed oxygen ($O_{ads}$). The ratio of ($O_{ads}/(O_{ads}+O_{latt})$) is about 0.42 for S-350, while it is 0.38 for S-550.

## 4. Conclusions

In summary, porous $Cu_2O$/CuO cubes with enhanced gas sensing performance were obtained by a precursor method. By the calcination of the precursor at different temperatures (350 °C, 450 °C and 550 °C), products with differences in the size, the surface area and the amount of $Cu_2O$ were obtained. The gas sensing properties of the products have been investigated systematically, and porous $Cu_2O$/CuO cubes exhibit higher sensing performance toward acetone than that of commercial CuO at lower operating temperature of 150 °C. Furthermore, S-350 gas sensor is the outstanding one in terms of response and response times due to the heterostructure of CuO and $Cu_2O$ and the higher surface area. And what's more, S-350 exhibits the better selectivity to acetone at 150 °C.

## Acknowledgements

This work is supported by the National Natural Science Foundation of China (21071060) and the National Basic Research Program of China (973 Program) (2013CB632403).

## References

[1] E. Eltzov, V. Pavluchkov, M. Burstin, R.S. Marks, Creation of a fiber optic based biosensor for air toxicity monitoring, Sensors and Actuators B 155 (2011) 859–867.
[2] X. Liu, S.T. Cheng, H. Liu, S. Hu, D.Q. Zhang, H.S. Ning, A survey on gas sensing technology, Sensors 12 (2012) 9635–9665.
[3] W.W. Guo, T.M. Liu, R. Sun, Y. Chen, W. Zeng, Z.C. Wang, Hollow, porous, and yttrium functionalized ZnO nanospheres with enhanced gas-sensing performances, Sensors and Actuators B 178 (2013) 53–62.
[4] K. Wang, T.Y. Zhao, G. Lian, Q.Q. Yu, C.H. Luan, Q.L. Wang, D.L. Cui, Room temperature CO sensor fabricated from Pt-loaded $SnO_2$ porous nanosolid, Sensors and Actuators B 184 (2013) 33–39.
[5] J.Y. Liu, T. Luo, F.L. Meng, K. Qian, Y.T. Wan, J.H. Liu, Porous hierarchical $In_2O_3$ micro-/nanostructures: preparation, formation mechanism, and their application in gas sensors for noxious volatile organic compound detection, Journal of Physical Chemistry C 114 (2010) 4887–4894.
[6] X.X. Zou, G.D. Li, P.P. Wang, J. Su, J. Zhao, L.J. Zhou, Y.N. Wang, J.S. Chen, A precursor route to single-crystalline $WO_3$ nanoplates with an uneven surface and enhanced sensing properties, Dalton Transactions 41 (2012) 9773–9780.
[7] J. Lee, D.H. Kim, S.H. Hong, J.Y. Jho, A hydrogen gas sensor employing vertically aligned $TiO_2$ nanotube arrays prepared by template-assisted method, Sensors and Actuators B 160 (2011) 1494–1498.
[8] L.L. Wang, T. Fei, Z. Lou, T. Zhang, Three-dimensional hierarchical flowerlike α-$Fe_2O_3$ nanostructures: synthesis and ethanol-sensing properties, ACS Applied Materials & Interfaces 3 (2011) 4689–4694.
[9] A. Taubert, F. Stange, Z.H. Li, M. Junginger, C. Guünter, M. Neumann, A. Friedrich, CuO nanoparticles from the strongly hydrated ionic liquid precursor (ILP) tetrabutylammonium hydroxide: evaluation of the ethanol sensing activity, ACS Applied Materials & Interfaces 4 (2012) 791–795.
[10] C. Yang, X.T. Su, F. Xiao, J.K. Jian, J.D. Wang, Gas sensing properties of CuO nanorods synthesized by a microwave-assisted hydrothermal method, Sensors and Actuators B 158 (2011) 299–303.
[11] X.L. Gou, G.X. Wang, J. Yang, J. Park, D.J. Wexler, Chemical synthesis, characterisation and gas sensing performance of copper oxide nanoribbons, Materials Chemistry 18 (2008) 965–969.
[12] Y.H. Choi, D.H. Kim, S.H. Hong, K.S. Hong, $H_2$ and $C_2H_5OH$ sensing characteristics of mesoporous p-type CuO films prepared via a novel precursor-based ink solution route, Sensors and Actuators B 178 (2013) 395–403.
[13] J.T. Zhang, J.F. Liu, Q. Peng, X. Wang, Y.D. Li, Nearly monodisperse $Cu_2O$ and CuO nanospheres: preparation and applications for sensitive gas sensors, Chemistry of Materials 18 (2006) 867–871.
[14] F.N. Meng, X.P. Di, H.W. Dong, Y. Zhang, C.L. Zhu, C.Y. Li, Y.J. Chen, Ppb $H_2S$ gas sensing characteristics of $Cu_2O$/CuO sub-microspheres at low-temperature, Sensors and Actuators B 182 (2013) 197–204.
[15] H.G. Zhang, Q.S. Zhu, Y. Zhang, Y. Wang, L. Zhao, B. Yu, One-pot synthesis and hierarchical assembly of hollow $Cu_2O$ microspheres with nanocrystals-composed porous multishell and their gas-sensing properties, Advanced Functional Materials 17 (2007) 2711–2766.
[16] S.Z. Deng, V. Tjoa, H.M. Fan, H.R. Tan, D.C. Sayle, M. Olivo, S. Mhaisalkar, J. Wei, C.H. Sow, Reduced graphene oxide conjugated $Cu_2O$ nanowire mesocrystals for high-performance $NO_2$ gas sensor, Journal of the American Chemical Society 134 (2012) 4905–4917.
[17] G.X. Zhu, H. Xu, Y.Y. Xiao, Y.J. Liu, A.H. Yuan, X.P. Shen, Facile fabrication and enhanced sensing properties of hierarchically porous CuO architectures, ACS Applied Materials & Interfaces 4 (2012) 744–751.
[18] H. Liu, X.W. Du, X.R. Xing, G.X. Wang, S.Z. Qiao, Highly ordered mesoporous $Cr_2O_3$ materials with enhanced performance for gas sensors and lithium ion batteries, Chemical Communications 48 (2012) 865–867.
[19] T. Tesfamichael, N. Motta, T. Bostrom, J.M. Bell, Development of porous metal oxide thin films by co-evaporation, Applied Materials & Interfaces 253 (2007) 4853–4859.
[20] Y.D. Wang, C.L. Ma, X.D. Sun, H.D. Li, Preparation of nanocrystalline metal oxide powders with the surfactant-mediated method, Inorganic Chemistry Communications 5 (2002) 751–755.
[21] H.L. Fernando, R.P. Geneva, D. Marauo, J.H. Louisa, Rapid preparation of high surface area iron oxide and alumina nanoclusters through a soft templating approach of sol-gel precursors, New Journal of Chemistry 37 (2013) 245–249.
[22] D.D. Han, X.Y. Jing, J. Wang, P.P. Yang, D.L. Song, J.Y. Liu, Porous lanthanum doped NiO microspheres for supercapacitor application, Journal of Electroanalytical Chemistry 682 (2012) 37–44.
[23] X.H. Liu, J. Zhang, Y.F. Kang, S.H. Wu, S.R. Wang, Brochantite tabular microspindles and their conversion to wormlike CuO structures for gas sensing, CrystEngComm 14 (2012) 620–625.
[24] H. Xu, G.X. Zhu, D. Zheng, C.Y. Xi, X. Xu, X.P. Shen, Porous CuO superstructure: precursor-mediated fabrication, gas sensing and photocatalytic properties, Journal of Colloid and Interface Science 383 (2012) 75–81.

[25] M. Birzescu, M. Niculescu, R. Dumitru, P. Budrugeac, E. Segal, Copper (II) oxalate obtained through the reaction of 1,2-ethanediol with $Cu(NO_3)_2{\cdot}3H_2O$, Journal of Thermal Analysis and Calorimetry 94 (2008) 297–303.
[26] H.G. Yu, J.G. Yu, S.W. Liu, S.H. Mann, Template-free hydrothermal synthesis of $CuO/Cu_2O$ composite hollow microspheres, Chemistry of Materials 19 (2007) 4327–4334.
[27] A. Katsifaras, N. Spanos, Effect of inorganic phosphate ions on the spontaneous precipitation of vaterite and on the transformation of vaterite to calcite, Journal of Crystal Growth 204 (1999) 183–190.
[28] R. Sahay, J. Sundaramurthy, P. SureshKumar, V. Thavasi, S.G. Mhaisalkar, S. Ramakrishna, Synthesis and characterization of CuO nanofibers, and investigation for its suitability as blocking layer in ZnO NPs based dye sensitized solar cell and as photocatalyst in organic dye degradation, Journal of Solid State Chemistry 186 (2012) 261–267.
[29] S. Anandan, G.J. Lee, J.J. Wu, Sonochemical synthesis of CuO nanostructures with different morphology, Ultrasonics Sonochemistry 19 (2012) 682–686.
[30] C.X. Wang, L.W. Yin, L.Y. Zhang, D. Xiang, R. Gao, Metal oxide gas sensors: sensitivity and influencing factors, Sensors 10 (2010) 2088–2106.
[31] X.L. Gou, G.X. Wang, J. Yang, J. Park, D. Wexler, Chemical synthesis, characterisation and gas sensing performance of copper oxide nanoribbons, Journal of Materials Chemistry 18 (2008) 965–969.
[32] X.X. Zou, G.D. Li, J. Zhao, P.P. Wang, Y.N. Wang, L.J. Zhou, J. Su, L. Li, J.S. Chen, Light-driven transformation of ZnS-cyclohexylamine nanocomposite into zinc hydroxysulfate: a photochemical route to inorganic nanosheets, Inorganic Chemistry 50 (2011) 9106–9113.
[33] T. Kimural, Y. Sekio, H. Nakamura, T. Siegrist, A.P. Raamirez, Cupric oxide as an induced-multiferroicwith high-Tc, Nature Materials 7 (2008) 291–294.
[34] G.X. Jin, K. Cao, G.C. Guo, L.X. He, Origin of ferroelectricity in high-Tc magnetic ferroelectric CuO, Physical Review Letters 108 (2012) 187205.
[35] L. Wang, K. Kalyanasundaram, M. Stanacevic, P. Gouma, Nanosensor device for breath acetone detection, Sensor Letters 8 (2010) 1–4.
[36] T.X. Fu, Research on gas-sensing properties of lead sulfide-based sensor for detection of $NO_2$ and $NH_3$ at room temperature, Sensors and Actuators B 140 (2009) 116–121.
[37] Z.H. Zhang, P. Wang, Highly stable copper oxide composite as an effective photocathode for water splitting via a facile electrochemical synthesis strategy, Journal of Materials Chemistry 22 (2012) 2456–2464.
[38] Z. Wang, Z.P. Qu, X. Quan, Z. Li, H. Wang, R. Fan, Selective catalytic oxidation of ammonia to nitrogen over $CuO–CeO_2$ mixed oxides prepared by surfactant-templated method, Applied Catalysis B: Environmental 134–135 (2013) 153–166.

## Biographies

**Li-Jing Zhou** received her BSc chemistry degree from Heibei North University, China, in 2009. Presently, she is a PhD student at State Key Laboratory of Inorganic Synthesis & Preparative Chemistry, Jilin University in China. She is now engaged in the synthesis of Cu-based materials and their application as gas sensors.

**Yong-Cun Zou** is a PhD student as State Key Laboratory of Inorganic Synthesis & Preparative Chemistry, Jilin University in China. He received his MSc from North East Normal University, China, in 2006.

**Jun Zhao** received her BSc chemistry degree from Changchun Institute of Technology, China, in 2006. She is currently undertaking her PhD at State Key Laboratory of Inorganic Synthesis & Preparative Chemistry, Jilin University in China with her major area of research being the characterization and gas sensing properties of $TiO_2$ and ZnO materials.

**Pei-Pei Wang** is a PhD student in State Key Laboratory of Inorganic Synthesis & Preparative Chemistry, Jilin University in China. Now, she is focused in the field of gas sensor.

**Liang-Liang Feng** she is a master student at State Key Laboratory of Inorganic Synthesis & Preparative Chemistry, Jilin University in China. Her research interest is synthesis of metal oxide mesoporous materials.

**Li-Wei Sun** received his BSc chemistry degree from Jilin University in China. He is currently undertaking his MSc at State Key Laboratory of Inorganic Synthesis & Preparative Chemistry, Jilin University in China. His research interests include synthesis and characterization of graphene oxide.

**De-Jun Wang** is a full professor of physical chemistry at College of Chemistry, Jilin University in China. He received his BSc (1977), MSc (1983) and PhD (1989) from Jilin University. His interests include photoelectric sensors, photocatalysts and related materials.

**Guo-Dong Li** is a full professor at State Key Lab of Inorganic Synthesis & Preparative Chemistry, College of Chemistry, Jilin University in China. He received his BSc (1995), MSc (1998) and PhD (2001) from Jilin University. His research interests include chemical sensors, lithium batteries, photocatalysts and other materials.